PAPER

Check for updates

Eco-friendly preparation and characterization of high-performance electrothermal graphene-AgNPs/lignocellulose composites†

Furong Liu, Cuiping Yu, [ID] * Xinyi Guo, Hui Peng and Shengqiang Qiu*

Graphene-based (Gr-based) electrothermal heaters, due to their light weight, low electrical resistance, high thermal conductivity, and easy accessibility, have attracted widespread attention in the field of electrothermal heating. To achieve a high steady-state temperature in electrothermal heaters under low voltage, here we constructed a Gr-based film with low electrical resistance. Firstly, we employed non-toxic vitamin C to reduce silver nitrate for the *in situ* chemical deposition of silver nanoparticles (AgNPs) on the Gr surface. The SEM results confirmed that the AgNPs were uniformly deposited on the Gr surface. The synergistic interaction between AgNPs and Gr provided high-speed electrons transport paths for the film. On the other hand, we employed biodegradable lignocellulose fiber (LCF) as a dispersant and film-forming agent. The aromatic ring structure of LCF interacts with Gr *via* π–π interactions, aiding the dispersion of Gr in aqueous solutions. SEM results revealed that LCF permeated through the surfaces and interstices of the two-dimensional Gr sheets, providing mechanical support for the composite film. This approach enables the creation of freestanding Gr-AgNPs/LCF electrothermal composites. The resistivity and electrothermal results demonstrated that the obtained 20 wt% Gr-based composite film possessed low electrical resistance (5.4 Ω sq^{-1}) and exhibited an outstanding saturated temperature of 214 °C under a very low input voltage of 7 V. The preparation method of this Gr-based composite film is simple, easy to operate, and environmentally friendly, providing a new reference for the preparation of eco-friendly and high-performance resistance heating electronics.

Introduction

Electrothermal composites are a class of functional resistors that utilize the Joule heating effect to convert the electrical energy into Joule heat. They are used in de-icers, defrosters, floor heating, and smart textiles, *etc.*[1–7] According to Joule's law: $Q = \dfrac{U^2}{R}t$, where Q is the heat creation, U is the applied voltage, t is the time, and R is the electrical resistance. To meet the safety requirements of low-voltage input for electric heaters, while ensuring high heating efficiency and saturation temperature,[1] it was necessary to maximally reduce the electrical resistance of the electrothermal composites. Additionally, to achieve rapid temperature response and uniform temperature distribution of the resistor, achieving high thermal conductivity in electric heaters can ensure their rapid heat dissipation and thermal transfer.[8] Traditional metallic electrothermal materials such as

Hunan Provincial Key Laboratory of Water Treatment Functional Materials, Hunan Province Engineering Research Center of Electroplating Wastewater Reuse Technology, College of Chemistry and Materials Engineering, Hunan University of Arts and Science, Changde 415000, PR China. E-mail: cpyu2018@huas.edu.cn; qshq915@163.com

† Electronic supplementary information (ESI) available. See DOI: https://doi.org/10.1039/d4ra00640b

Ni–Cr composite metals,[9] copper,[10] and indium tin oxide[11] have been widely used due to their excellent electrical conductivity. However, their application is limited due to large weight, poor mechanical properties, slower response rates, and susceptibility to acid and alkali corrosion.

Compared with traditional metal electrothermal materials, carbon-based heaters are considered potential substitutes due to their lighter weight, higher thermal conductivity, lower resistivity, enhanced energy conversion efficiency, resistance to acid and alkali corrosion, and accessibility.[1,12–14] Particularly, graphene (Gr) exhibits theoretical electrical conductivity as high as 6000 S cm^{-1} and thermal conductivity reaching up to 5300 W m^{-1} K^{-1}.[15–17] The monolayer sp^2 hybridized nanostructure provides high-speed transmission channels for electrons and phonons, endowing Gr films with exceptional electrothermal properties.[18] For example, Cheng *et al.*[17] fabricated electrothermal composites using functionalized Gr and carbon black. Their study revealed that functionalized Gr significantly enhanced the electrothermal performance of the composite films. The highest heating rate achieved was 5.6 °C s^{-1}, with the maximum steady-state temperature reaching up to 83 °C, both markedly surpassing the performance of the composite films in the control group without functionalized Gr. Ma *et al.*[19] produced Gr/carbon paper electrothermal composites with

rapid electrothermal heating rate ($215 \, °C \, s^{-1} \, V^{-1}$). At an input voltage of 1.75 V, the highest steady-state temperature reached 235 °C, surpassing the performance of commercial Gr heater. Although Gr films exhibited exceptional electrothermal properties, their fabrication process was complex, required sophisticated equipment, and was energy-intensive. To achieve higher saturation temperatures and faster heating efficiency at lower voltages for Gr-based electric heaters, utilizing the synergistic effect of nano-fillers and employing green and simple process conditions to reduce the electrical resistance of Gr films is an effective method for enhancing their electrothermal performance. Liang et al.[18] utilized multi-walled carbon nanotubes (MWCNT) and reduced graphene oxide (RGO) as composite fillers, which were mixed and dispersed with cationic cellulose, followed by vacuum filtration to form a film. The filler content was fixed at 40 wt%, and the effect of the synergistic interaction on the electrothermal performance was investigated by varying the mass ratio of MWCNT to RGO. The study found that the composite film exhibited optimal electrothermal heating performance when the MWCNT to RGO mass ratio was 35 : 5. At an applied voltage of 18 V, the steady-state temperature exceeded 102.15 °C, indicating a significant synergistic effect of the two fillers.

Silver nanoparticles (AgNPs) exhibit high electrical conductivity ($6.3 \times 10^7 \, S \, m^{-1}$) and can form micro-nano synergistic conductive networks in conjunction with two-dimensional Gr.[20,21] The stacking and contact of these two materials on and within a polymer matrix can create more continuous and compact paths for heat conduction and electrical conduction, leading to enhanced electrothermal effects. For example, Nie et al.[22] constructed micro-channels on a transparent PET surface, and then filled these channels with commercially available Gr and AgNPs using the blade coating method to form a transparent electrothermal film. The AgNPs bridged the Gr sheets, facilitating the enhancement of electrothermal performance. This composite film achieved a steady-state temperature exceeding 70 °C under a 3 V voltage, and exhibited good flexibility. However, the fabrication process involved in this work was complex, and the organic plastic matrix was difficult to degrade. The contact between AgNPs and Gr sheets was achieved through physical dispersion rather than in situ chemical deposition, resulting in high contact resistance. Hydrazine hydrate,[23] $NaBH_4$,[24–26] N,N'-dimethylformamide,[27] and sodium citrate[28] have been used for the chemical deposition of AgNPs on the Gr surface.

Based on the above analysis, this work employed a simple stirring and mixing method to in situ chemically deposit AgNPs on the surface of Gr using non-toxic vitamin C (VC). Additionally, lignocellulosic fiber (LCF) was selected as the matrix for the electrothermal composites. The primary reason for choosing LCF was: LCF predominantly found in the byproducts of the papermaking industry, offer sustainable and biodegradable sources, rendering them an eco-friendly material. Furthermore, LCF is characterized by its aromatic ring structures and quinone groups, contributing to its hydrophobic nature. This property facilitated the dispersion of Gr in aqueous solutions. Additionally, the one-dimensional linear architecture of LCF allowed

it to interpenetrate with two-dimensional Gr sheets, thereby providing mechanical support structures. The loading of AgNPs onto the Gr surface enriched the conductive network between the Gr layers. Under the synergistic effect of the AgNPs and Gr, the electrical conductivity of the electrothermal composite film was further enhanced. The entire preparation process was environmentally friendly, green, and straightforward, providing a novel reference for the fabrication of eco-friendly, high-performance, Gr-based electric-thermal films.

Experimental

Materials

Graphene (purity > 99%) was supplied by Suzhou Carbonfeng Graphene Technology Co., Ltd (China). Lignocellulosic fiber utilized in the experiment, with 1–2 mm in length and 5–20 μm in diameter, were supplied by Jinzhou Baoyi Building Materials Technology Co., Ltd (China). Silver nitrate ($AgNO_3$) and L-ascorbic acid were purchased from Sinopharm Chemical Reagent Co., Ltd (China). All chemicals were analytical grade and were used as received without further treatment.

Preparation of Gr-AgNPs/LCF composites

To assess the influence of Gr-AgNPs content on the electrothermal behavior of composite films, the mass ratio of Gr to AgNPs was fixed at 4 : 1.[28,29] Under this condition, the impact on electrothermal properties was explored by altering the weight ratio of Gr-AgNPs to LCF. To prepare 7.5 wt% Gr-AgNPs/LCF composite, 0.03 g of Gr was added into 15 mL of deionized (DI) water at 25 °C followed by ultrasonication for 30 min (200 W output power). Then, 0.4625 g of LCF was mixed with the Gr dispersion through sonication for 20 min. The uniform Gr/LCF dispersion was acquired. Subsequently, 12 mg $AgNO_3$ was added to the above Gr/LCF dispersion, and ultrasonic-mixing was performed for 20 min. To reduce $AgNO_3$ to form AgNPs, 12 mg of VC was introduced to the above dispersion and sonicated for 10 min, followed by mechanical stirring for 12 h. The Gr-AgNPs/LCF dispersion was filtered to obtain Gr-AgNPs/LCF cake. Finally, the composite cake was dried at 80 °C for 5 h and called Gr-AgNPs/LCF. Samples of other concentrations (10 wt%, 15 wt%, 20 wt%) were prepared using the same procedure.

Characterization

The chemical features of Gr, LCF, and Gr-AgNPs/LCF composites were characterized via Fourier transform infrared (FTIR; Nicolet iS5, Thermo Fisher Scientific) analyses performed within the range of 4000 to 500 cm^{-1}. X-ray diffraction (XRD; DX-2700) patterns were conducted with the scan rate of $0.2° \, s^{-1}$ from 10° to 80° (2θ) (Cu Kα radiation, $\lambda = 1.5408$ Å). The cross-sectional morphologies of Gr-AgNPs/LCF composites were acquired using a scanning electron microscope (SEM; Regulus 8100, Hitachi) operating at an acceleration voltage of 3 kV. The elemental mappings of the Gr-AgNPs/LCF composites were assessed using energy-dispersive X-ray spectroscopy (EDS), coupled with SEM, operating at an acceleration voltage of 20 kV.

X-ray photoelectron spectroscopy (XPS) analysis of 20 wt% Gr-AgNPs/LCF was conducted using a Thermo Scientific K-Alpha spectrometer, equipped with Al Kα source. The measurements were performed at a filament current of 6 mA and an accelerating voltage of 12 kV. To obtain the square resistance values of the samples, a M-3 Mini type four-probe tester was used. The average value was calculated from five distinct regions on each composite film to ensure accuracy. The external power supply used to record the voltage–power–temperature values of the samples was an A-BF adjustable direct current (DC) power supply (SP-305). A digital thermometer with range of −50–200 °C (LCD-281S) was used to record the temperature. Electro-thermal films with an effective heating area of approximately 4 cm² (2 cm × 2 cm) were fabricated by precision cutting. Copper strips were adhered to the designated area of the electrothermal films to serve as electrodes for testing purposes. The sample test setup was illustrated in Fig. S1.†

Results and discussion

Gr-AgNPs/LCF composite films with excellent electrothermal properties were prepared using the method shown in Fig. 1. AgNO₃ was reduced by VC to form AgNPs and coated on the surface of Gr,[30,31] two-dimensional Gr sheets were constructed to overlap and form conductive paths, the zero-dimensional AgNPs acted as a bridge between the sheets, and the one-dimensional LCF acted as a dispersion agent and provided mechanical support for the composite films. Through the synergistic effect of Gr and AgNPs, the resistance of the composite films was further reduced, and the electrothermal performance of the composite films were significantly improved. 20 wt% Gr-AgNPs/LCF composite film still exhibited excellent flexibility.

FTIR was performed on the samples to obtain information on the functional groups and structural compositions of LCF
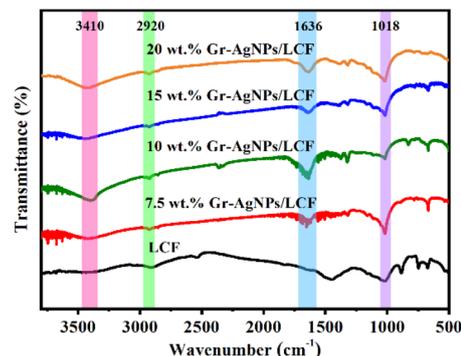

Fig. 2 FTIR spectrums of LCF and Gr-AgNPs/LCF composites.

and Gr-AgNPs/LCF composite films. As shown in Fig. 2, the broad absorption peak at 3410 cm⁻¹ was caused by the phenolic and aliphatic hydroxyl groups of the LCF side chain,[32] the absorption peak at 2920 cm⁻¹ was attributed to the absorption vibration peaks of methyl and methylene groups in LCF,[33,34] the absorption peak at 1636 cm⁻¹ was due to the C=C stretching vibrations of the typical aromatic rings of LCF,[35,36] the absorption peak at 1018 cm⁻¹ was assigned to the C–O stretching vibrations of methoxy, aliphatic secondary alcohols and ethers in LCF,[37] and the absorption peaks at 1636 cm⁻¹ and 1018 cm⁻¹ were typical characteristic infrared absorption peaks of LCF. These peaks were clearly observed in the composite films with the four filler contents. The peak position did not move significantly compared with that of LCF, and essentially no new absorption peaks were observed, indicating that no new chemical bond was formed between Gr-AgNPs and LCF.

As shown in Fig. 3, the XRD pattern of the Gr-AgNPs/LCF composites showed obvious sharp peaks at 38.2°, 44.2°, 64.3°, and 77.3°, corresponding to the characteristic absorption peaks at the (111), (200), (220), and (311) planes of the face centred
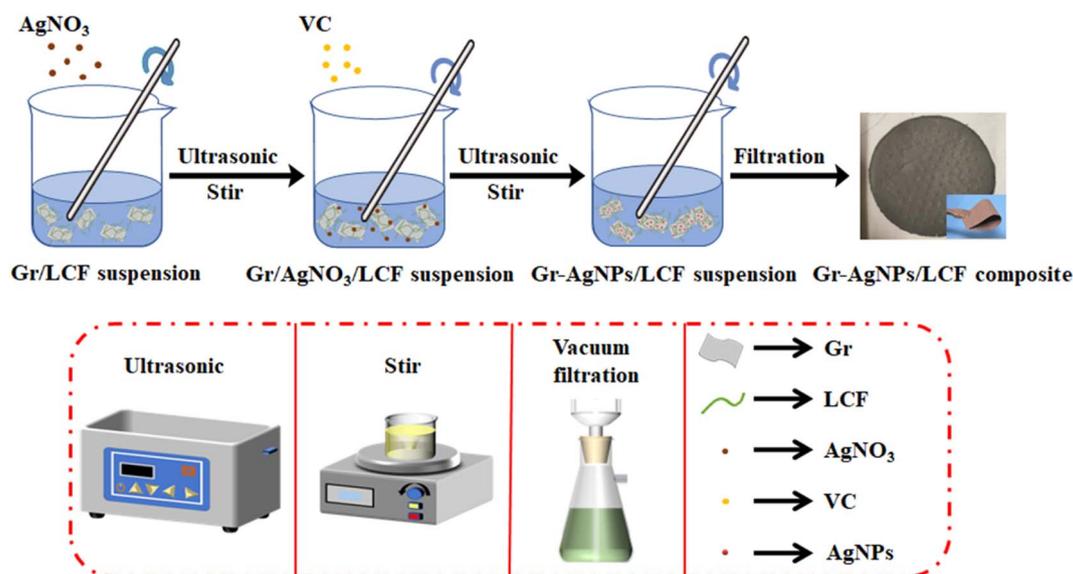

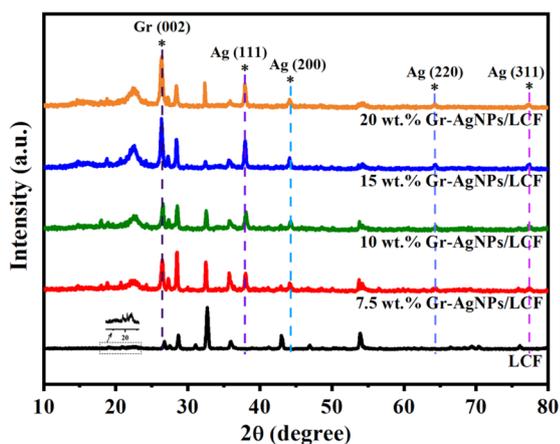Fig. 1 Preparation of Gr-AgNPs/LCF composites.

Fig. 3 XRD curves of LCF and Gr-AgNPs/LCF composites.

cubic Ag phase (JCPDS No. 87-0720), respectively,[18,38,39] which strongly confirmed that AgNO$_3$ was successfully reduced to Ag in the composite films. A high-resolution spectrum of Ag 3d, as depicted in Fig. S2,† exhibited peaks at 368.1 eV and 374.1 eV, corresponding to the Ag 3d$_{5/2}$ and Ag 3d$_{7/2}$ levels, respectively. This conclusively confirmed the complete reduction of Ag$^+$ to Ag^0. The diffraction peak at 26.3° was the (002) characteristic diffraction peak of Gr. With increasing filler content, both the area and intensity of this diffraction peak were markedly enhanced.[40,41] The interlayer spacing of Gr calculated using the Bragg formula was approximately 0.34 nm, which was accordance with the previous study.[42–44] LCF is primarily composed of lignin, cellulose, and hemicellulose. Considering that lignin and hemicellulose are primarily amorphous in nature, the diffraction peak about 22.5° was ascribed to lignin and hemicellulose. Other diffraction peaks evident in Fig. 3 for the LCF were predominantly ascribed to cellulose. Specifically, the diffraction peak observed around 26.8° corresponded to the
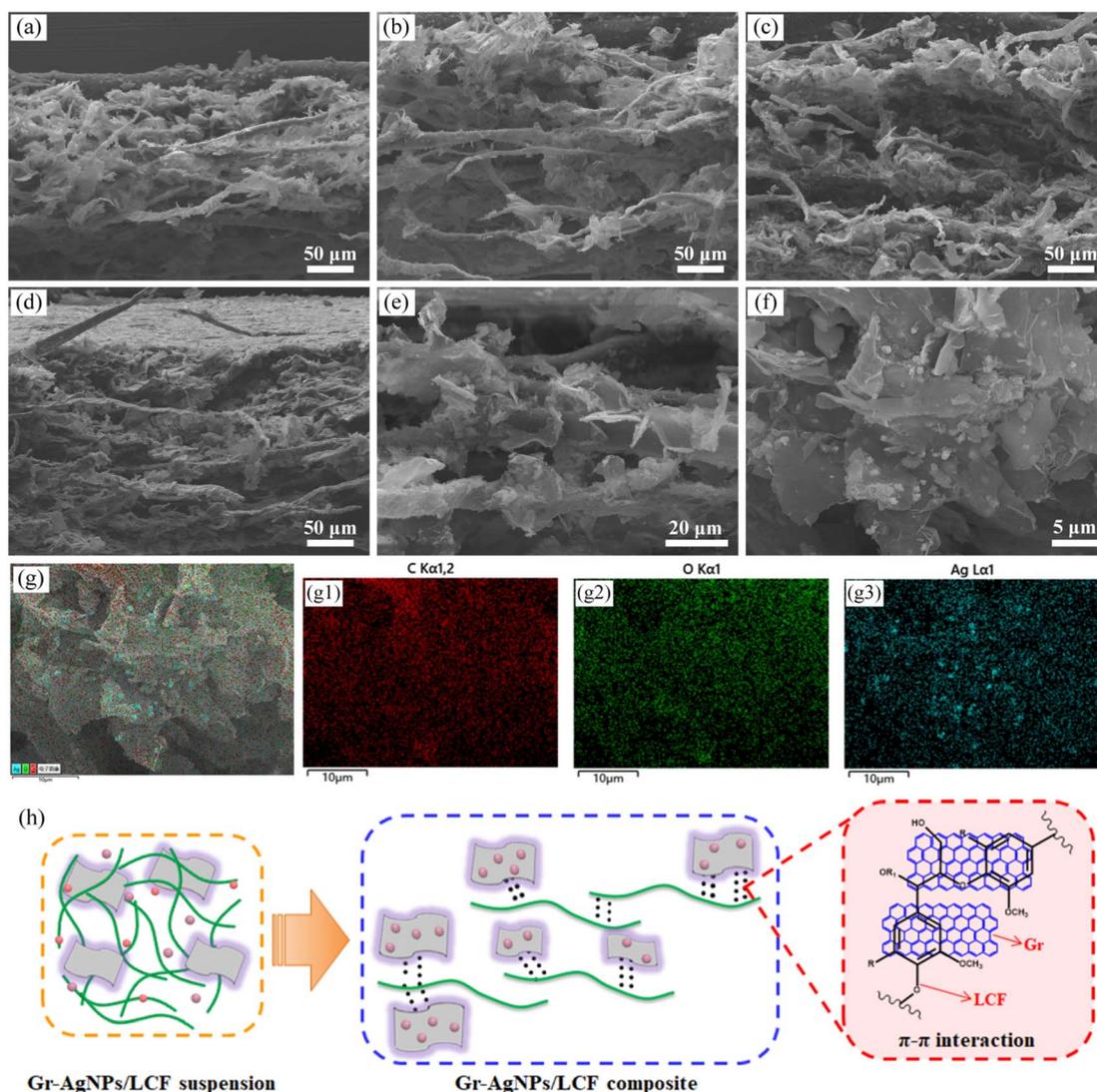

Fig. 4 SEM images of (a and e) 7.5 wt%, (b) 10 wt%, (c) 15 wt%, and (d and f) 20 wt% of Gr-AgNPs/LCF composites, (g, g1, g2 and g3) EDS mapping of 20 wt% Gr-AgNPs/LCF composite, (h) Schematic diagram of Gr-AgNPs/LCF architectures.

(002) crystal plane, signifying the interchain stacking in cellulose. The peaks detected at 32.7° and 43.0° could be attributed to the (040) and (004) crystal planes, respectively.[45,46] Compared to the original LCF, the peak intensities at 32.7° and 43.0° of the Gr-AgNPs/LCF composites were significantly reduced, which could be attributed to the rearrangement of hydrogen bonds between cellulose molecular chains due to the presence of VC and water.[47–49] Simultaneously, an increase in the peak intensity at 22.5° was observed, indicating an augmentation in the amorphous regions within the composite films. This phenomenon could be attributed to a decrease in the degree of orderliness of the cellulose, accompanied by an increase in the relative peak intensities of lignin and hemicellulose. The comparison of the characteristic peak positions of the composites with four filler contents showed no obvious shifts, indicating that the structure of Gr-AgNPs/LCF has not changed.

As shown in Fig. 4a–d, most of LCF extended in an in-plane horizontal orientation, forming the foundational skeleton of the composite films. This structure offered robust mechanical support. The Gr sheet was wrinkled, indicating that the Gr used in this experiment was thin. And the sheet was complete and undamaged, reflecting its high quality.[50] Gr sheets adhered closely to the surface of LCF, forming a tight interface (Fig. 4e). This adherence could be attributed to the π–π interactions between Gr and LCF,[51–53] as well as the hydrophobic effects of both Gr and LCF, facilitating the dispersion of Gr in aqueous solutions with the assistance of LCF. In the fabricated composites, obvious AgNPs were detected on the surface of the Gr sheet with a uniform distribution (Fig. 4f and g), further confirming that the AgNPs were successfully synthesized in the composites, which was consistent with the XRD and XPS characterization results. The diameters of the AgNPs were
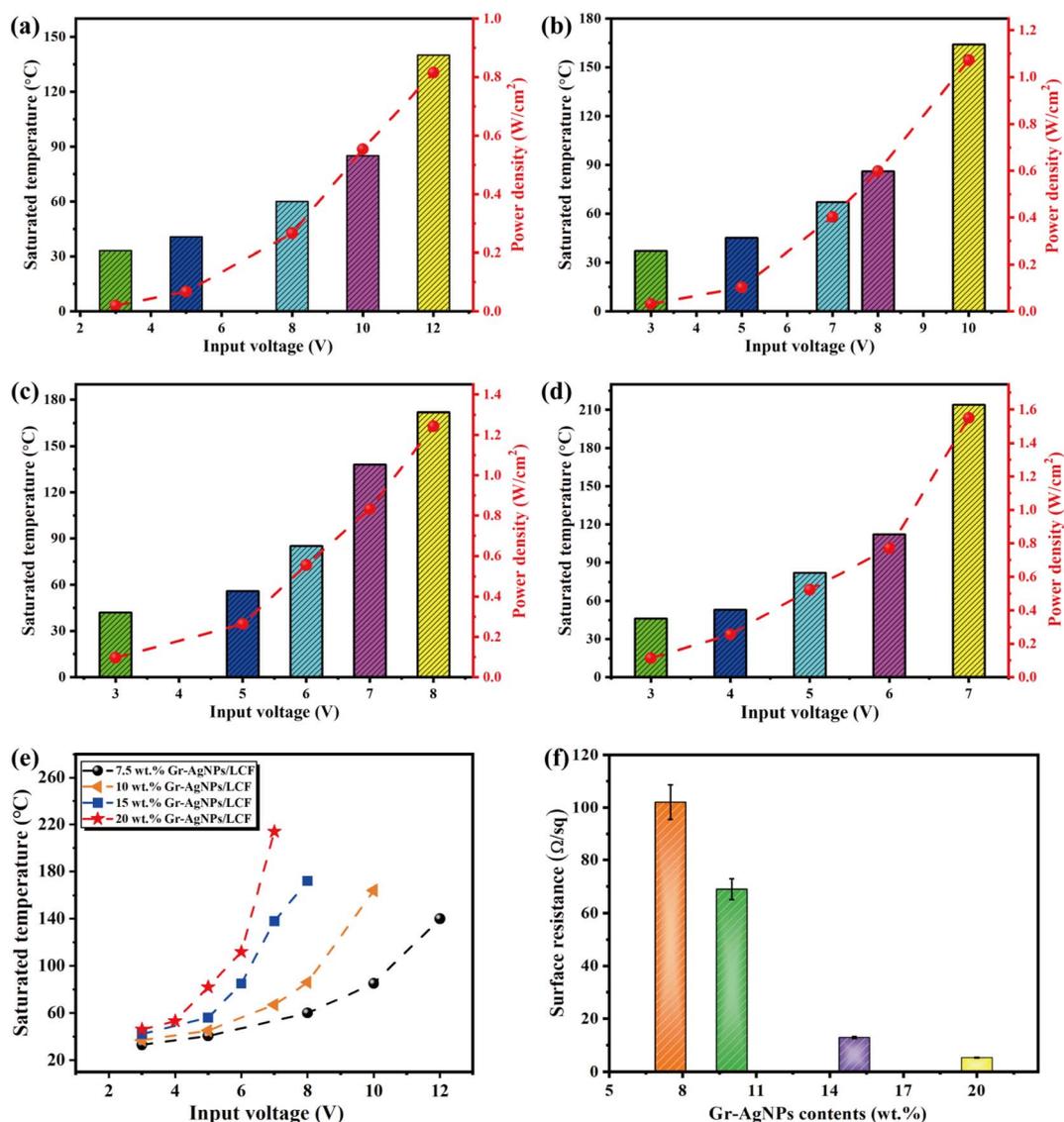

Fig. 5 Voltage–power density-saturated temperature histogram of (a) 7.5 wt%, (b) 10 wt%, (c) 15 wt%, (d) 20 wt% of Gr-AgNPs/LCF composites. (e) Saturated temperature of Gr-AgNPs/LCF composites with various filler loadings under different input voltage. (f) Sheet resistance of Gr-AgNPs/LCF composites.

Table 1 Comparison of electrothermal performance of 20 wt% Gr-AgNPs/LCF and other Gr-contained electrothermal materials[a]

Material	Gr content	Driving voltage (V)	Steady-state temperature (°C)	Ref.
Chemically reduced GO	100 wt%	3.2	42	55
Electrochemically exfoliated Gr	100 wt%	30	139	56
Gr/microsphere/bamboo fiber	27 wt%	7	80	57
GO/CNT/AlN	23.6 wt%	4.5	131	58
Gr/MWCNT/CB	22 wt%	10	165	59
Gr/f-MWCNT/CB	26 wt%	3	175	60
POSS-Gr/MWCNT	38 vol%	15	188	61
Gr/PPy/Juncus effusus	17 wt%	10	147	62
Thermally reduced GO/PU	20 wt%	22	75	63
Thermally reduced GO/epoxy	15 wt%	10	120	64
Gr-AgNPs/LCF	16 wt%	7	214	This work

[a] GO represents graphene oxide; CNT represents carbon nanotube; AlN represents aluminium nitride; CB represents carbon black; f-MWCNT represent acid treated MWCNTs; POSS-Gr represents POSS functionalized graphene; PPy represents polypyrrole; PU represents polyurethane.

approximately 550 nm (Fig. S3†). The synergistic interaction between Gr and AgNPs further enhanced the electrical and thermal conductivity of the composite films, thereby improving the electrothermal properties of the material. The schematic diagram of the Gr-AgNPs/LCF architectures was presented in Fig. 4h. LCF comprises lignin, which is abundant in aromatic rings, thereby facilitating π–π interactions with Gr.[51,52,54] This attribute promoted a close contact between LCF and Gr, enhancing their interfacial adhesion.

At room temperature, the electrothermal behavior of the Gr-AgNPs/LCF composite films was investigated by varying the constant voltage. Fig. 5a–d illustrated the variation in steady-state temperature and power density of the composite films with different Gr-AgNPs contents (7.5 wt%, 10 wt%, 15 wt%, 20 wt%) in response to the changes in input voltage. The heating power density could be calculated using the equation $P_s = \dfrac{U^2}{R \times S}$, where R and S denoted the resistance and area of the composite films, respectively. For a given composite film, the power density increased with an increase in voltage, indicating that the electric heating performance could be controlled by adjusting the voltage. Under the same voltage, composite films with a higher Gr-AgNPs content exhibited a higher power density due to their relatively lower resistance. Fig. 5e illustrated the trend of steady-state temperature variation with input voltage for Gr-AgNPs/LCF composite films at different filler contents. The steady-state temperature of each composite film monotonically increased with the increment of voltage. At a specific voltage, as the Gr-AgNPs content increased, the steady-state temperature of the composite film rose. This could be attributed to the lower resistance of the composite film, allowing for a higher power density and consequently a higher steady-state temperature. Additionally, the increased Gr-AgNPs content enhanced the electrical and thermal conductivity of the composite film, aligning with the results of electrical conductivity tests. As depicted in Table 1, compared to previously reported Gr electrothermal heaters, the composite films prepared in this study demonstrated a higher steady-state temperature at a lower voltage. At a low driving voltage of 7 V,

with an input power density of 1.55 W cm^{-2}, the highest steady-state temperature achieved was 214 °C. At a temperature of 214 °C, the 20 wt% Gr-AgNPs/LCF electrothermal film was exposed to a room-temperature air environment with a continuous input voltage of 7 V for 1 h. The steady-state temperature of the electrothermal film consistently remained at approximately 214 °C, indicating its stability at high temperatures (Fig. S4†).

The sheet resistance of the samples was tested to understand the electrical conductivity of the samples, and the results were shown in Fig. 5f. The sheet resistances of Gr-AgNPs/LCF composites with Gr-AgNPs contents of 7.5 wt%, 10 wt%, 15 wt%, and 20 wt% were 102.1 Ω sq^{-1}, 69.3 Ω sq^{-1}, 12.9 Ω sq^{-1}, and 5.4 Ω sq^{-1}, respectively, indicating that the sheet resistance of the composite material decreased sharply with increasing Gr-AgNPs content. This phenomenon potentially occurred because an increased Gr-AgNPs content increased the number of electron transport paths. In addition, the bridging effect of AgNPs between Gr sheets further increased the electron transport paths of the composite films, ensuring the continuous conduction of electrons.[65] The lower sheet resistance was beneficial for improving the electrothermal performance of the composite films.

Conclusions

In this study, AgNPs were *in situ* chemically deposited onto the surface of Gr *via* the reduction of silver nitrate using VC, achieving uniform coverage of the AgNPs. Utilizing LCF, which are widely sourced and easily degradable, as a dispersant and film-forming agent, we have developed a self-supporting and flexible Gr-AgNPs/LCF composite film. When the content of Gr-AgNPs was 20 wt%, at a low driving voltage of 7 V and an input power density of 1.55 W cm^{-2}, the composite film reached a maximum steady-state temperature of 214 °C. This was attributed to the ultra-low sheet resistance of 5.4 Ω sq^{-1}, allowing for higher steady-state temperatures due to the higher power density. This study provided a new reference for the preparation of novel, environmentally friendly, high-performance Gr-based electrothermal heaters.

Conflicts of interest

The authors declare that they have no known competing financial interests or personal relationships that could have appeared to influence the work reported in this paper.

Acknowledgements

References

1 D. Janas and K. K. Koziol, *Nanoscale*, 2014, **6**, 3037–3045.

2 N. Karim, M. Zhang, S. Afroj, V. Koncherry, P. Potluri and K. S. Novoselov, *RSC Adv.*, 2018, **8**, 16815–16823.

3 J. Fan, Z. Long, J. Wu, P. Gao, Y. Wu, P. Si and D. Zhang, *J. Coat. Technol. Res.*, 2023, **20**, 1557–1568.

4 H. Ba, L. Truong-Phuoc, T. Romero, C. Sutter, J.-M. Nhut, G. Schlatter, G. Giambastiani and C. Pham-Huu, *Carbon*, 2021, **182**, 655–668.

5 Y. Cui, Z. Jiang, G. Zheng, W. Wang, M. Zhou, P. Wang, Y. Yu and Q. Wang, *Chem. Eng. J.*, 2022, **446**, 137189.

6 X. Zhang, D. Li, K. Liu, J. Tong and X. Yi, *Int. J. Lightweight Mater. Manuf.*, 2019, **2**, 241–249.

7 R. Wang, Z. Xu, J. Zhuang, Z. Liu, L. Peng, Z. Li, Y. Liu, W. Gao and C. Gao, *Adv. Electron. Mater.*, 2017, **3**, 1600425.

8 T. Y. Zhang, H. M. Zhao, D. Y. Wang, Q. Wang, Y. Pang, N. Q. Deng, H. W. Cao, Y. Yang and T. L. Ren, *Nanoscale*, 2017, **9**, 14357–14363.

9 R. F. Kopf, R. Melendes, D. C. Jacobson, A. Tate, M. A. Melendes, R. R. Reyes, R. A. Hamm, Y. Yang, J. Frackoviak, N. G. Weimann, H. L. Maynard and C. T. Liu, *J. Vac. Sci. Technol. B*, 2002, **20**, 871–875.

10 Z. Zhao, C. Yan, D. Li, X. Tang, J. Ran, S. Bi, D. Cheng, G. Cai and X. Wang, *Surf. Interfaces*, 2023, **36**, 102600.

11 R. Gupta, K. D. M. Rao, S. Kiruthika and G. U. Kulkarni, *ACS Appl. Mater. Interfaces*, 2016, **8**, 12559–12575.

12 D. Janas and K. K. Koziol, *Carbon*, 2013, **59**, 457–463.

13 J. Luo, H. Lu, Q. Zhang, Y. Yao, M. Chen and Q. Li, *Carbon*, 2016, **110**, 343–349.

14 D. Sui, Y. Huang, L. Huang, J. Liang, Y. Ma and Y. Chen, *Small*, 2011, **7**, 3186–3192.

15 A. A. Balandin, S. Ghosh, W. Bao, I. Calizo, D. Teweldebrhan, F. Miao and C. N. Lau, *Nano Lett.*, 2008, **8**, 902–907.

16 A. A. Balandin, *Nat. Mater.*, 2011, **10**, 569–581.

17 Y. Zhao, M. Niu, F. Yang, Y. Jia and Y. Cheng, *Eng. Sci.*, 2019, **8**, 33–38.

18 S. Liang, H. Wang and X. Tao, *J. Mater. Res. Technol.*, 2022, **17**, 2388–2399.

19 H. Chang, Y. Jia, L. Xiao, H. Chen, K. Zhao, Y. Chen and Y. Ma, *Carbon*, 2019, **154**, 150–155.

20 A. Mohammadpour-Haratbar, Y. Zare and K. Y. Rhee, *J. Mater. Res. Technol.*, 2022, **18**, 4894–4902.

21 L. Zheng, G. Zhang, M. Zhang, S. Guo and Z. H. Liu, *J. Power Sources*, 2012, **201**, 376–381.

22 B. Nie, H. Song, B. Lv, X. Xiong, G. Qi, Y. Zhang, J. Qiu, X. Li, J. Shao and Z. Wei, *J. Mater. Chem. C*, 2023, **11**, 6145–6154.

23 R. Pasricha, S. Gupta and A. K. Srivastava, *Small*, 2009, **5**, 2253–2259.

24 J. Shen, M. Shi, N. Li, B. Yan, H. Ma, Y. Hu and M. Ye, *Nano Res.*, 2010, **3**, 339–349.

25 Y. J. Qiao, J. Kang, C. Q. Song, N. Zhou, P. Zhang and G. F. Song, *RSC Adv.*, 2024, **14**, 2621–2632.

26 X. Zhu, H. Liu, Y. Wu, J. Ye, Y. Li and Z. Liu, *RSC Adv.*, 2022, **12**, 25906–25911.

27 S. Liu, J. Tian, L. Wang and X. Sun, *J. Nanopart. Res.*, 2011, **13**, 4539–4548.

28 W. Yuan, Y. Gu and L. Li, *Appl. Surf. Sci.*, 2012, **261**, 753–758.

29 R. Gao, N. Hu, Z. Yang, Q. Zhu, J. Chai, Y. Su, L. Zhang and Y. Zhang, *Nanoscale Res. Lett.*, 2013, **8**, 32.

30 M. U. Rashid, M. K. H. Bhuiyan and M. E. Quayum, *Dhaka Univ. J. Pharm. Sci.*, 2013, **12**, 29–33.

31 K. S. Hui, K. N. Hui, D. A. Dinh, C. H. Tsang, Y. R. Cho, W. Zhou, X. Hong and H. H. Chun, *Acta Mater.*, 2014, **64**, 326–332.

32 X. Wang, Y. Qu, L. Jiao, H. Bian, R. Wang, W. Wu, G. Fang and H. Dai, *Compos. Sci. Technol.*, 2021, **204**, 108641.

33 J. Saleem, M. Z. K. Baig, U. B. Shahid, S. Mansour and G. McKay, *Energy Rep.*, 2022, **8**, 117–123.

34 S. Ayub, B. H. Guan, H. Soleimani, F. Ahmad, Z. U. Nisa, J. Y. Yusuf, M. A. B. Hamid and Y. M. Hassan, *Ain Shams Eng. J.*, 2023, **14**, 101996.

35 M. Deshpande, S. Sundararajan, A. B. Samui and P. S. Kulkarni, *J. Energy Storage*, 2021, **35**, 102338.

36 S. S. Panesar, S. Jacob, M. Misra and A. K. Mohanty, *Ind. Crops Prod.*, 2013, **46**, 191–196.

37 L. Sánchez-López, B. Chico, I. Llorente, M. Escudero, R. Lozano and M. García-Alonso, *Mater. Chem. Phys.*, 2022, **287**, 126296.

38 M. R. Vengatesan, E. Alhseinat, A. F. Arangadi, S. Anwer, Y. Y. Kannangara, J.-K. Song and F. Banat, *Sep. Purif. Technol.*, 2019, **229**, 115799.

39 E. S. Madivoli, S. I. Wanakai, P. K. Kairigo and R. S. Odhiambo, *Materials*, 2023, **16**, 4271.

40 J. Zhao, C. Wang, C. Wang, K. Zhang, B. Cong, L. Yang, X. Zhao and C. Chen, *J. Appl. Polym. Sci.*, 2023, **140**, e53401.

41 X. Liang and F. Dai, *ACS Appl. Mater. Interfaces*, 2020, **12**, 3051–3058.

42 D. Jiao, N. Song, P. Ding and L. Shi, *Compos. Commun.*, 2022, **31**, 101101.

43 D. An, Z. Li, H. Chen, C. Liang, Z. Sun, J. Li, J. Yao, Y. Liu and C. Wong, *Composites, Part A*, 2022, **156**, 106890.

44 T. Zhou, C. Wu, Y. Wang, A. P. Tomsia, M. Li, E. Saiz, S. Fang, R. H. Baughman, L. Jiang and Q. Cheng, *Nat. Commun.*, 2020, **11**, 2077.

45 H. Zhao, J. Kwak, Z. Conradzhang, H. Brown, B. Arey and J. Holladay, *Carbohydr. Polym.*, 2007, **68**, 235–241.

46 S. H. Kim, C. M. Lee and K. Kafle, *Korean J. Chem. Eng.*, 2013, **30**, 2127–2141.

47 B. Lindman, B. Medronho, L. Alves, C. Costa, H. Edlund and M. Norgren, *Phys. Chem. Chem. Phys.*, 2017, **19**, 23704–23718.

48 R. Alqus, S. J. Eichhorn and R. A. Bryce, *Biomacromolecules*, 2015, **16**, 1771–1783.

49 S. P. S. Chundawat, G. Bellesia, N. Uppugundla, L. da Costa Sousa, D. Gao, A. M. Cheh, U. P. Agarwal, C. M. Bianchetti, G. N. Phillips Jr, P. Langan, V. Balan, S. Gnanakaran and B. E. Dale, *J. Am. Chem. Soc.*, 2011, **133**, 11163–11174.

50 D. Lee, B. Lee, K. H. Park, H. J. Ryu, S. Jeon and S. H. Hong, *Nano Lett.*, 2015, **15**, 1238–1244.

51 W. O. S. Doherty, P. Mousavioun and C. M. Fellows, *Ind. Crops Prod.*, 2011, **33**, 259–276.

52 V. K. Thakur, M. K. Thakur, P. Raghavan and M. R. Kessler, *ACS Sustainable Chem. Eng.*, 2014, **2**, 1072–1092.

53 A. Kumar and G. A. Kumar, *Radiat. Phys. Chem.*, 2023, **202**, 110562.

54 R. Wang, H. Bian, H. Ji and R. Yang, *Cellulose*, 2018, **25**, 6139–6149.

55 Y. Guo, C. Dun, J. Xu, J. Mu, P. Li, L. Gu, C. Hou, C. A. Hewitt, Q. Zhang, Y. Li, D. L. Carroll and H. Wang, *Small*, 2017, **13**, 1702645.

56 C. Li, Y.-T. Xu, B. Zhao, L. Jiang, S.-G. Chen, J.-B. Xu, X.-Z. Fu, R. Sun and C.-P. Wong, *J. Mater. Sci.*, 2016, **51**, 1043–1051.

57 Z.-H. Tang, W.-B. Zhu, J.-Z. Chen, Y.-Q. Li, P. Huang, K. Liao and S.-Y. Fu, *Nano Mater. Sci.*, 2023, **5**, 319–328.

58 Z. Huang, S. Li, H. Guo, C. Huang, Y. Bian, Y. Gong, J. Huang and Q. Zeng, *J. Mater. Chem. C*, 2023, **11**, 9925–9936.

59 Y. Liu, X. Ma, H. Zhang, J. Sun, J. Qian and X. Wang, *ACS Appl. Electron. Mater.*, 2022, **4**, 814–822.

60 Y. Liao, Y. Tian, X. Ma, M. Zhao, J. Qian and X. Wang, *ACS Appl. Mater. Interfaces*, 2020, **12**, 48077.

61 W. Zhang, Y. Xu, J. Ma, J. He, H. Ye, J. Song, Y. Chen and L. Xu, *ACS Appl. Mater. Interfaces*, 2023, **15**, 4430–4440.

62 J. Gong, W. Tang, L. Xia, Z. Fu, S. Zhou, J. Zhang, C. Zhang, L. Li, H. Ji and W. Xu, *Chem. Eng. J.*, 2023, **452**, 139338.

63 E. Owji, F. Ostovari and A. Keshavarz, *Phys. Scr.*, 2022, **97**, 105704.

64 D. Zhang, S. Yang, S. Zhang, W. Liu, H. Pan, X. Bai, M. Ma, Y. Shang and P. Li, *ACS Appl. Eng. Mater.*, 2023, **1**, 1535–1542.

65 Y. Zhou, J. Yang, X. Cheng, N. Zhao, L. Sun, H. Sun and D. Li, *Carbon*, 2012, **50**, 4343–4350.